Nuclear Engineering and Technology 55 (2023) 3039–3045

Contents lists available at ScienceDirect

Nuclear Engineering and Technology

journal homepage: www.elsevier.com/locate/net

Original Article

Health monitoring of carbon fiber-reinforced polymer composites in γ-radiation environment using embedded fiber Bragg grating sensors

Jing Zhong [a], Feida Chen [a, c, *], Yuehao Rui [a], Yong Li [b], Xiaobin Tang [a, c, *]

[a] Department of Nuclear Science and Technology, Nanjing University of Aeronautics and Astronautics, Nanjing, 211106, China
[b] College of Materials Science and Technology, Nanjing University of Aeronautics and Astronautics, Nanjing, 211106, China
[c] Key Laboratory of Nuclear Technology Application and Radiation Protection in Astronautics, Ministry of Industry and Information Technology, Nanjing, 211106, China

ARTICLE INFO

Article history:
Received 27 May 2022
Received in revised form
7 September 2022
Accepted 18 April 2023

Keywords:
Fiber-reinforced polymer (FRP) composites
Gamma radiation
Health monitoring
Fiber Bragg grating (FBG)

ABSTRACT

Fiber-reinforced polymer (FRP) composites are considered suitable candidates for structural materials of spacecrafts due to their excellent properties of high strength, light weight, and corrosion resistance. An online health monitoring method for FRP composites must be applied to space structures. However, the application of existing health monitoring methods to space structures is limited due to the harsh space environment. Here, carbon fiber-reinforced polymer (CFRP) composites embedded with fiber Bragg grating (FBG) sensors were prepared to explore the feasibility of strain monitoring using embedded FBG sensors in γ-radiation environment. The analysis of the influence of radiation on the strain monitoring demonstrated that the embedded FBG can be successfully applied to the health monitoring of FRP composites in radiation environment.

1. Introduction

Fiber-reinforced polymer (FRP) composites are commonly used in the aerospace, automotive, and construction industries due to their superior properties of light weight, high strength, corrosion endurance, fatigue resistance, and strong designability [1–5]. Hence, FRP composites demonstrate high potential as structural materials for spacecrafts. However, the space environment where spacecrafts operate can significantly degrade the properties of FRP composites because of its extremely harsh characteristics of high vacuum, thermal cycles, atomic oxygen, ultraviolet light, radiation, and presence of space debris [6–8]. FRP composites exposed to the space environment suffer from strength change, interface debonding, surface cracking, brittle fracture, molecular chain breakage, and other types of damage [9–16]. Thus, an effective health monitoring method for FRP composites is crucial to ensure their long-term reliability in service.

Numerous health monitoring methods for FRP composites, such as ultrasonic detection radiographic inspection, acoustic emission monitoring, strain gauge testing, and optical fiber detection, have been proposed [17–25]. Although ultrasonic and radiographic inspection methods are mature and widely used, they can only be utilized for offline testing. Frequent deboning of the interface between piezoelectric sensors and composites in acoustic emission inspections introduces noise during the propagation process of elastic waves in materials. Strain gauge sensors are easily embedded in composite materials, but their electrical signals are susceptible to electromagnetic interference. By contrast, optical fiber Bragg grating (FBG) sensors have attracted considerable research attention in the field of damage detection due to their embeddability, anti-electromagnetic interference capabilities and characteristics of wavelength encoded. Previous studies verified the feasibility of the embedded FBG sensor technique in dynamic stress monitoring, thermal cycle detection, and thermal deformation measurement [26–30]. However, the harsh environment may also exert some effect on the monitoring method itself. When FBG sensors are applied to radiation environment for sensing, it was found that high-energy ionizing radiation can cause signals drifting and transmission loss to FBGs, which can introduce errors for the sensing of temperature or strain [31–33]. On the basis, relevant studies have focused on improving the radiation resistance of FBGs mainly by fiber composition modulation, grating inscription techniques and pre-processing method to mitigate the effects of

* Corresponding authors. Department of Nuclear Science and Technology, Nanjing University of Aeronautics and Astronautics, Nanjing, 211106, China.
E-mail addresses: fdchen@nuaa.edu.cn (F. Chen), tangxiaobin@nuaa.edu.cn (X. Tang).

https://doi.org/10.1016/j.net.2023.04.028

radiation on FBGs [34–36]. However, it is still unknown whether FBG sensors are capable for materials monitoring in radiation environments.

In this work, FBG sensors were embedded in FRP composites for strain monitoring of materials in γ-radiation environment. The quantitative model of the relationship between FBG wavelength shift and FRP strain was established, and the relationship between FBG wavelength and temperature was determined. Moreover, the irradiation experiment proves that the compatibility between FBG and FRP materials maintains well after irradiation and the coefficients of strain sensitivity of FBG sensors embedded in FRP composites are slightly affected by the radiation. Hence, the embedded FBG is very suitable for materials monitoring in radiation environments.

2. Working principle of FBG

FBG sensor is an optical fiber with a regular distribution of grating. The grating is inscribed inside the fiber core via exposure to ultraviolet light or femtosecond laser. The refractive index of optical fiber varies periodically at a certain length. Notably, FBG is a kind of superior bandpass filter that can reflect a narrow spectrum of incident light and transmit the rest at the same time [37]. The structure schematic is shown in Fig. 1. Bragg wavelength (λ_B) is the central wavelength in the reflection spectrum of FBG and defined as follows:

$$\lambda_B = 2n_e\Lambda, \tag{1}$$

where n_e is the effective refractive index of the optical fiber core and Λ is the period of Bragg grating. Temperature and strain can affect n_e and Λ and further lead to shifting in λ_B.The wavelength shift subjected to strain and temperature is expressed as follows:

$$\Delta\lambda_B = K_\varepsilon\Delta\varepsilon + K_T\Delta T, \tag{2}$$

where $\Delta\lambda_B$, $\Delta\varepsilon$, and ΔT represent the shift of λ_B, strain, and temperature, respectively; K_ε and K_T are coefficients of strain and temperature sensitivity, respectively, which are related to parameters of fiber and grating [38]. The wavelength shift is linearly proportional to the variation in temperature and strain to ensure that strain and temperature can be monitored by FBG.

3. Experiments

3.1. Selection of FBG sensors

For the reliable strategy for monitoring and sensing in radiation environments, FBG sensors with resistance to radiation should be selected properly. Currently, the FBGs written on pure silica fibers or F-doped fibers are considered to be of low radiation sensitivity, which present lower radiation loss and wavelength shift than that written on the standard Ge-doped fibers [39–41]. Additionally, FBGs fabricated with femtosecond laser developed in recent years, compared to the conventional UV laser inscription technique, show better high-temperature stability and better resistance to radiation-induced wavelength shift [42–45]. Here, the resistance to radiation and commercial access of various types of FBG sensors have been taken into comprehensive consideration. In this study, FBG sensors inscribed onto pure silica fiber SM1250SC(9/125)P (FemtoFiberTec, Germany) with good resistance to radiation were selected. The FBGs were written by femtosecond laser point-by-point writing technique and with a polyimide coating and a grating length of 4 mm.

3.2. Specimen manufacturing

Carbon fiber-reinforced polymer (CFPR) laminates in this study were manufactured using the mold pressing technique with unidirectional carbon fiber/epoxy prepreg USN15000/7901/RC33(Guangwei Composites Co., China). The dimensions of specimen were 90 mm × 13 mm × 2 mm (length × width × thickness) according to the ASTM D7264 standard. The stacking sequence was $[0_4/90_4/0_4/90_4/0_4]$. FBG sensors were located between the third and fourth prepreg layers along the direction of the carbon fiber, that is, $[0_3/FBG/0/90_4/0_4/90_4/0_4]$. The ends of FBG sensors were taken out from the side of the laminate, inserted into the Teflon tube, and sealed with silicone rubber to prevent the optical fiber from breaking due to the curing of the resin. The schematic of the FBG embedded in CFRP composites is shown in Fig. 2. The temperature in the curing process was raised from room temperature to 80 °C at 1 °C/min, maintained for 0.5 h, increased to 120 °C at 1 °C/min, and held for 1.5 h with a pressure of 12 MPa. Finally, the laminates were cooled to room temperature naturally.

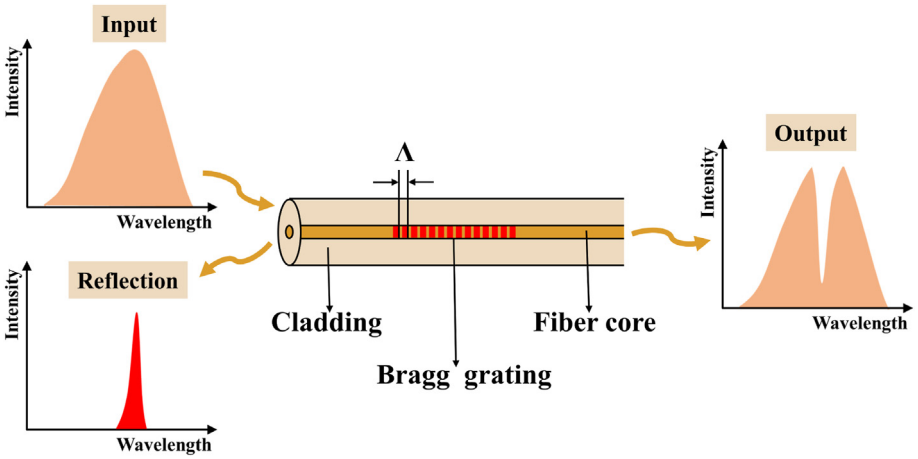

Fig. 1. Structure schematic of the FBG sensor consisting of cladding, fiber core, and Bragg grating. The regular distribution of grating allows the reflection of a narrow spectrum of incident light.

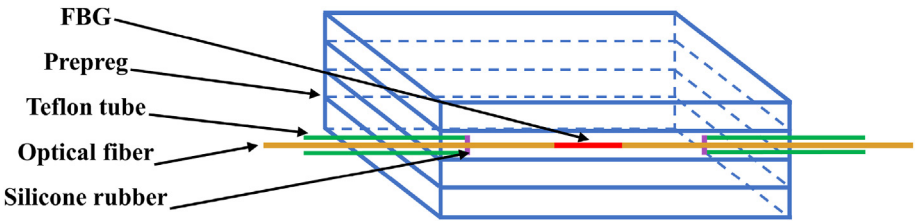

Fig. 2. Schematic of the FBG embedded in CFRP composites.

3.3. Measurement of the coefficient of strain sensitivity

Coefficients of strain sensitivity were detected with a mechanical testing machine WDW-100 (WANCE, China) under three-point flexural loading. The reflected signals of FBG sensors were recorded using an FBG demodulator SuperHawk 6000 (Hope-Excellence Information Technology Co., China). As shown in Fig. 3, the specimen embedded with FBG was secured on the fixture with the margin of FBG connected to the wavelength demodulator, and the demodulator was connected to a laptop. The loading speed was controlled at 1 mm/min.

3.4. Effects of temperature on FBG sensors

FBG sensors were placed in a high-low-temperature test chamber for measuring their response to the temperature range of 0 °C-50 °C. Coefficients of temperature sensitivity of FBG before and after being embedded in CFRP were measured. The initial temperature was set to 50 °C, and the next temperature decreased in gradients of 10 °C. The temperature was stabilized for 30 min after each adjustment, and wavelength data were recorded.

3.5. γ-radiation experiments

A ^{60}Co γ-radiation facility (Nanjing University of Aeronautics and Astronautics Irradiation Center) was employed as the radiation resource. Embedded FBGs and free FBGs are presented in Fig. 4 and Table 1, where "E" and "F" represent embedded FBGs and free FBGs, respectively. All the grating of free and embedded FBGs are not bare, which are covered with a polyimide coating. Free FBGs were attached to the acrylic plate with polyimide tape to prevent wavelength interference due to optical fiber bending. The irradiation time were 10, 20 30, 49, 69, and 98 h. The irradiation dose rate was 10.19 kGy/h, and irradiation doses were 101.9, 203.8, 305.7, 499.3, 703.1, and 998.6 kGy, which were calibrated with a silver dichromate dosimeter. Wavelength data of FBG sensors were recorded at 30 °C after each dose of irradiation.

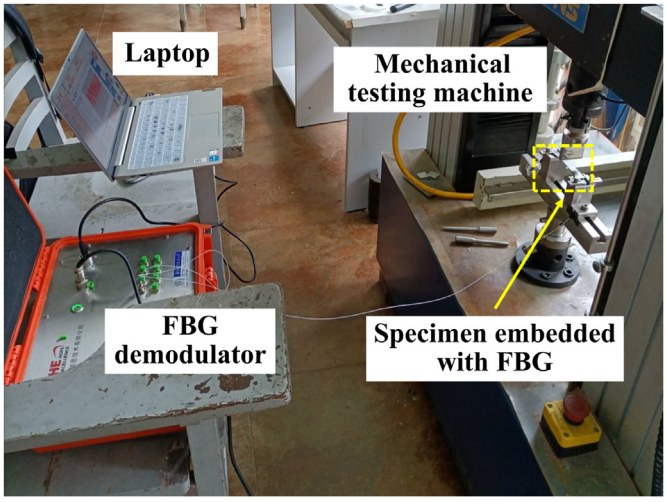

Fig. 3. Experimental setup for testing the coefficient of strain sensitivity.

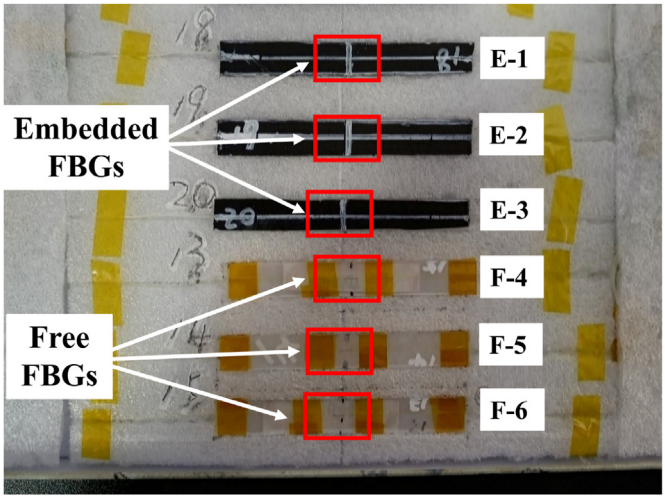

Fig. 4. Photos of embedded FBGs and free FBGs ("E" and "F" represent embedded FBGs and free FBGs, respectively).

Table 1
FBG sensors in this work ("E" and "F" represent embedded FBGs and free FBGs, respectively).

FBG label	1	2	3	4	5	6
Embedded/Free	E	E	E	F	F	F

4. Results and discussion

4.1. Coefficients of strain sensitivity of FBG sensors

The linear relationship between wavelength shift and the applied load is illustrated in Fig. 5a, in which data are normalized to the unloaded wavelength. The linear fitting curves of the wavelength shift versus applied strain are shown in Fig. 5b, which refers to the strain of composites rather than FBG sensors. Slopes of curves, that is coefficients of strain sensitivity (K_ε), are listed in Table 2. The mechanical deformation and photoelastic effect result in the wavelength shift of FBG under load. In addition, the linear response of wavelength to strain reflects the satisfactory compatibility of embedded FBGs and composites. Curves of wavelength versus strain will change abruptly because the strain that transfers to FBG becomes uneven if FBG is delaminated with composites.

4.2. Effects of temperature on FBG sensors

The wavelength shift of free FBGs with temperature is shown in

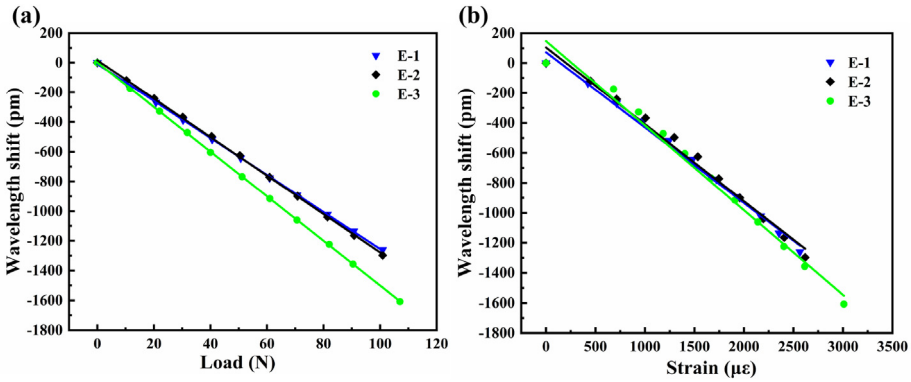

Fig. 5. Response of FBG sensors with applied strain. Relationship between the (a) wavelength of FBGs embedded in the CFRP and load and (b) wavelength shift of embedded FBGs and applied strain ("E" represents the embedded FBG).

Table 2
Coefficients of strain sensitivity for embedded FBGs ("E" represents embedded FBG).

FBG label	E-1	E-2	E-3
K_ε (pm/με)	−0.503	−0.513	−0.564

Table 3
Coefficients of temperature sensitivity of FBGs before and after being embedded in the CFRP in this work.

FBG label	E-1	E-2	E-3	F-4	F-5	F-6
K_T before being embedded (pm/°C)	10.2	10.4	10.1	10.4	9.9	10.2
K_T after being embedded (pm/°C)	12.8	11.4	11.8	–	–	–

Fig. 6a, in which data are normalized to the wavelength at 0 °C. The wavelength shift of FBGs demonstrated a positive linear relationship with temperature due to thermal expansion and thermo-optic effect. Besides, thermal deformation of CFRP also affects the wavelength of FBGs when FBGs are embedded in composites. The response of FBG to temperature before and after being embedded in CFRP is displayed in Fig. 6b. K_T values for each FBG used in this work are listed in Table 3. According to the slope of the fitting curve, the coefficient of temperature sensitivity of FBG increases after being embedded in CFRP because the thermal expansion of CFRP leads to the additional strain exerted on FBG. Furthermore, the wavelength shift attributed to the thermal strain of CFRP was obtained when the wavelength shift of the free FBG was subtracted from that of the embedded FBG. The thermal strain of CFRP is insignificant in the temperature range of 0 °C-50 °C. The interference of temperature on strain measurement via FBG can be corrected on the basis of the linear relationship between the temperature and FBG wavelength.

4.3. Effects of radiation on FBG sensors

The curves of wavelength shift versus temperature and applied strain after a γ-irradiation dose of 998.6 kGy are depicted in Fig. 7 to investigate the effects of radiation on FBG sensors. As illustrated in Fig. 7a, the wavelength shift is still linearly proportional to the applied strain. Therefore, the FBG sensors remain well bonded to the materials after irradiation. K_ε values of embedded FBGs after irradiation are listed in Table 4. Although K_ε of each FBG varies slightly after a γ-irradiation dose of 998.6 kGy, the value is negligible and within the experimentally allowed error range. Thus, the FBG sensor is suitable for internal strain sensing of CFRP in radiation environments. The curves of wavelength shift versus temperature are shown in Fig. 7b. K_T values of free and embedded FBGs after a γ-irradiation dose of 998.6 kGy are listed in Table 5. K_T of each FBG also changes slightly after irradiation.

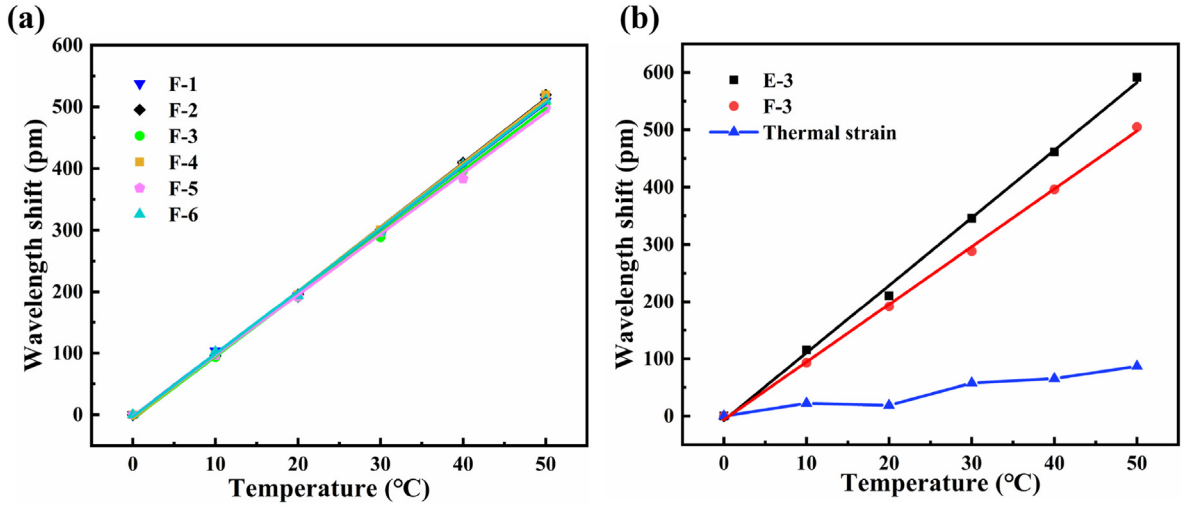

Fig. 6. Response of FBG sensors to ambient temperature. (a) Relationship between wavelength shift of free FBGs and temperature and (b) comparison of temperature sensitivity measured by the FBG before and after being embedded in CFRP ("E" and "F" represent embedded FBG and free FBG, respectively).

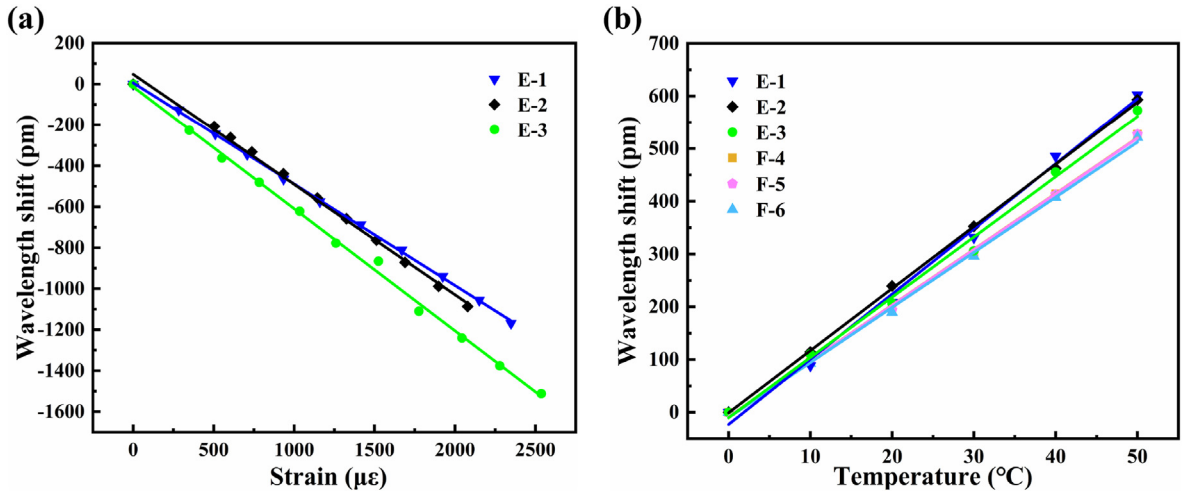

Fig. 7. Relationship between the wavelength of FBG and strain and temperature after a γ-irradiation dose of 998.6 kGy. (a) Applied strain and (b) temperature ("E" and "F" represent embedded FBG and free FBG, respectively).

Table 4
Coefficients of strain sensitivity for embedded FBGs after a γ-irradiation dose of 998.6 kGy ("E" represents embedded FBG).

FBG label	E-1	E-2	E-3
K_ε after irradiation (pm/με)	−0.495	−0.539	−0.596

Table 5
Coefficients of temperature sensitivity for free and embedded FBGs after a γ-irradiation dose of 998.6 kGy ("E" and "F" represent embedded FBGs and free FBGs, respectively).

FBG label	E-1	E-2	E-3	F-4	F-5	F-6
K_T after irradiation (pm/°C)	12.4	11.8	11.4	10.8	10.6	10.5

4.4. Practical application in the monitoring of radiation-induced strain

The wavelength shift of FBGs is presented in Fig. 8a, including three embedded FBGs and three free FBGs, in the γ-radiation dose range of 0–998.6 kGy. The wavelength of three embedded FBGs raises as the irradiation dose increases. Meanwhile, the wavelength shift of three free FBGs after irradiation was also confirmed, given that the refractive index of the quartz material is influenced by high-energy rays. This phenomenon will lead to errors in the monitoring of the FBG wavelength. This work considered that the effect of radiation on the wavelength of embedded FBG lies in two aspects. On one hand, the direct effect of γ-radiation on the FBG itself leads to a wavelength shift. On the other hand, the internal strain of composites develops after irradiation, thereby altering the wavelength of FBG.

In this study, the free FBGs were set as a control group to test the wavelength shift caused by the direct effect of γ radiation on FBGs. To eliminate the direct effect of radiation on FBG sensors, the average wavelength shift of three free FBGs was subtracted from the wavelength shift of each embedded FBG, thus the wavelength shift of FBG induced by the internal strain of composites was obtained, as shown in Fig. S1. The internal strain of composites induced by γ irradiation was further obtained according to Eq. (2) and K_ε value in Table 4. The radiation-induced strain versus irradiation dose for three embedded FBGs is presented in Fig. 8b. The radiation-induced strain increases with the increase of irradiation,

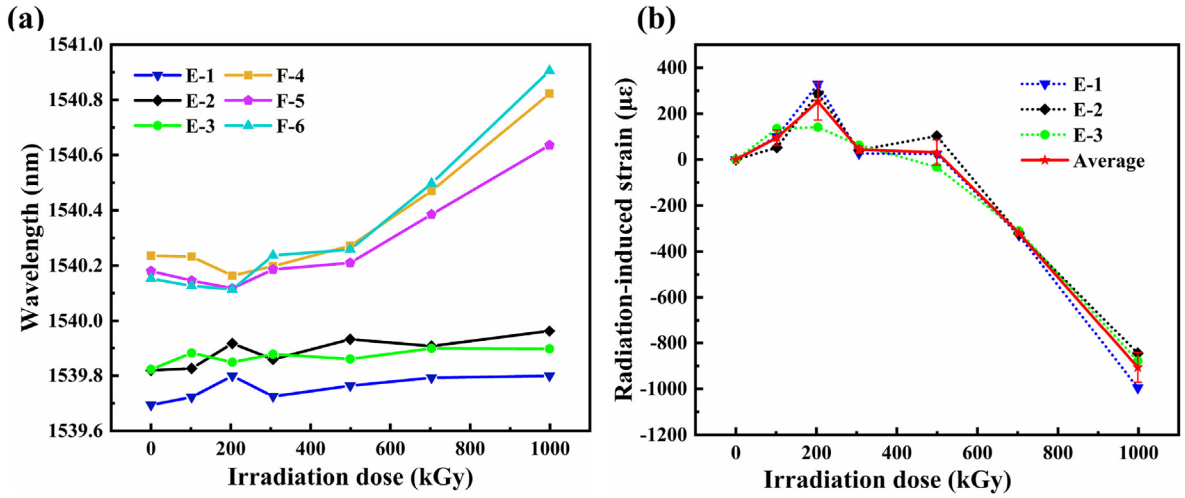

Fig. 8. Monitored radiation-induced strain of CFRP in the γ-irradiation dose of 0–988.6 kGy. (a) Wavelength monitored by free and embedded FBGs and (b) radiation-induced strain of CFRP monitored by embedded FBGs ("E" and "F" represent embedded FBG and free FBG, respectively).

which reaches a maximum when the irradiation dose is 203.8 kGy. However, the radiation-induced strain decreases with the continuous increase of irradiation dose. The radiation-induced strain becomes a negative value and further increases in reverse as the irradiation dose increases until it reaches 499.3 kGy. The average radiation-induced strain of CFRP monitored by FBG is 906.2 με after exposure to an irradiation dose of 998.6 kGy.

5. Conclusion

A monitoring technique based on embedded FBG was developed in this study to assess the health status of CFRP composites in γ-radiation environment. The quantitative model of the relationship between the FBG wavelength shift and CFRP strain was established. The relationship between the temperature and FBG wavelength shift was determined to correct the influence of temperature on strain measurement. Furthermore, this work demonstrated the negligible effect of radiation on coefficients of strain sensitivity and verified the applicability of the FBG method in radiation environment. The relationship of material strain monitored by FBG versus the radiation dose was acquired in the irradiation dose range of 0–988.62 kGy. In summary, strain detection based on FBG is an effective health monitoring method for evaluating CFRP composites exposed to radiation environment. This work provides a feasible strategy for the nondestructive evaluation of health status of CFRP composites in radiation environment. Meanwhile, a future investigation can focus on determining whether or not the effect of high-dose radiation on the coefficient of strain sensitivity of FBG is negligible. In addition, with the development of new fabrication techniques, it is expected that FBG sensors with excellent resistance to radiation will be commercially available in the near future. And their low radiation-induced wavelength shift will contribute to superiority for strain sensing in radiation environment.

Declaration of competing interest

The authors declare that they have no known competing financial interests or personal relationships that could have appeared to influence the work reported in this paper.

Acknowledges

The authors would like to thank Hongquan Liu, Jiaqi Shi, and Yifan Yang of Nanjing University of Aeronautics and Astronautics for the help in materials preparation. In addition, this work was supported by Postdoctoral Research Foundation of China (Grant No.2020M671488), the Fundamental Research Funds for the Central Universities (Grant No. NS2021036), and Postgraduate Research & Practice Innovation Program of NUAA (Grant No. xcxjh20210622).

Appendix A. Supplementary data

Supplementary data to this article can be found online at https://doi.org/10.1016/j.net.2023.04.028.

References

[1] G. Xian, R. Guo, C. Li, Combined effects of sustained bending loading, water immersion and fiber hybrid mode on the mechanical properties of carbon/glass fiber reinforced polymer composite, Compos. Struct. 281 (2022), 115060.
[2] T.K. Das, P. Ghosh, N.C. Das, Preparation, development, outcomes, and application versatility of carbon fiber-based polymer composites: a review, Adv. Compos. Hybrid Mater. 2 (2019) 214–233.
[3] D.D.L. Chung, Processing-structure-property relationships of continuous carbon fiber polymer-matrix composites, Mater. Sci. Eng.: R: Rep. 113 (2017) 1–29.
[4] F. Akman, H. Ogul, I. Ozkan, M.R. Kaçal, O. Agar, H. Polat, K. Dilsiz, Study on gamma radiation attenuation and non-ionizing shielding effectiveness of niobium-reinforced novel polymer composite, Nucl. Eng. Technol. 54 (2022) 283–292.
[5] W. Ramadan, K. Sakr, M. Sayed, N. Maziad, N. El-Faramawy, Investigation of acrylic/boric acid composite gel for neutron attenuation, Nucl. Eng. Technol. 52 (2020) 2607–2612.
[6] J. Jang, S. Hong, J. Kim, N. Goo, W. Yu, Accelerated testing method for predicting long-term properties of carbon fiber-reinforced shape memory polymer composites in a low earth orbit environment, Polymers. 13 (2021) 1628.
[7] L. Wang, F. Zhang, Y. Liu, γ-rays radiation resistant shape memory cyanate ester resin and its composites with high transition temperature, Smart Mater. Struct. 28 (2019), 075039.
[8] M. Nishida, A. Hongo, Y. Hiraiwa, M. Higashide, Effects of gamma ray irradiation on penetration hole in and fragment size from carbon fiber reinforced composite plates in hypervelocity impacts, Compos. B Eng. 169 (2019) 229–238.
[9] R. Pastore, A. Delfini, M. Albano, A. Vricella, M. Marchetti, F. Santoni, F. Piergentili, Outgassing effect in polymeric composites exposed to space environment thermal-vacuum conditions, Acta Astronaut. 170 (2020) 466–471.
[10] J.H. Jang, S.B. Hong, J. Kim, N.S. Goo, H. Lee, W. Yu, Long-term properties of carbon fiber-reinforced shape memory epoxy/polymer composites exposed to vacuum and ultraviolet radiation, Smart Mater. Struct. 28 (2019), 115013.
[11] L. Zheng, L. Wang, Z. Wang, L. Wang, Effects of γ-ray irradiation on the fatigue strength, thermal conductivities and thermal stabilities of the glass fibres/epoxy resins composites, Acta Metall. Sin. 31 (2018) 105–112.
[12] D. Sekulic, M.M. Stevanovic, Effects of gamma irradiation and post-irradiation annealing on carbon/epoxy UDC properties deduced by methods of local loading, J. Nucl. Mater. 412 (2011) 190–194.
[13] Z.X. Wu, J.W. Li, C.J. Huang, R.J. Huang, L.F. Li, Effect of gamma irradiation on the mechanical behavior, thermal properties and structure of epoxy/glass-fiber composite, J. Nucl. Mater. 441 (2013) 67–72.
[14] L. Liu, L. Feng, T. Ma, Z. Xu, X. Pei, Y. Liu, H. Shi, Y. Tang, L. Liu, H. Deng, C. Wang, Mechanical properties, thermal stability and microstructure evolution of carbon fiber-reinforced epoxy composites exposed to high-dose γ-rays, Radiat. Phys. Chem. 194 (2022), 110056.
[15] R. Li, Y. Gu, Z. Yang, M. Li, S. Wang, Z. Zhang, Effect of γ irradiation on the properties of basalt fiber reinforced epoxy resin matrix composite, J. Nucl. Mater. 466 (2015) 100–107.
[16] E.N. Hoffman, T.E. Skidmore, Radiation effects on epoxy/carbon-fiber composite, J. Nucl. Mater. 392 (2009) 371–378.
[17] S. Hassani, M. Mousavi, A.H. Gandomi, Structural health monitoring in composite structures: a comprehensive review, Sensors. 22 (2022) 153.
[18] S. Goossens, F. Berghmans, Z. Sharif Khodaei, F. Lambinet, E. Karachalios, D. Saenz-Castillo, T. Geernaert, Practicalities of BVID detection on aerospace-grade CFRP materials with optical fibre sensors, Compos. Struct. 259 (2021), 113243.
[19] C. Tuloup, W. Harizi, Z. Aboura, Y. Meyer, K. Khellil, R. Lachat, On the use of in-situ piezoelectric sensors for the manufacturing and structural health monitoring of polymer-matrix composites: a literature review, Compos. Struct. 215 (2019) 127–149.
[20] A. Wronkowicz, K. Dragan, K. Lis, Assessment of uncertainty in damage evaluation by ultrasonic testing of composite structures, Compos. Struct. 203 (2018) 71–84.
[21] S. Sikdar, D. Liu, A. Kundu, Acoustic emission data based deep learning approach for classification and detection of damage-sources in a composite panel, Compos. B Eng. 228 (2022), 109450.
[22] L. Grassia, M. Iannone, A. Califano, A. D'Amore, Strain based method for monitoring the health state of composite structures, Compos. B Eng. 176 (2019), 107253.
[23] O. Ahmed, X. Wang, M. Tran, M. Ismadi, Advancements in fiber-reinforced polymer composite materials damage detection methods: towards achieving energy-efficient SHM systems, Compos. B Eng. 223 (2021), 109136.
[24] O. Rifaie-Graham, E.A. Apebende, L.K. Bast, N. Bruns, Self-reporting fiber-reinforced composites that mimic the ability of biological materials to sense and report damage, Adv. Mater. 30 (2018), 1705483.
[25] R. Di Sante, Fibre optic sensors for structural health monitoring of aircraft composite structures: recent advances and applications, Sensors. 15 (2015) 18666–18713.
[26] J. Frieden, J. Cugnoni, J. Botsis, T. Gmür, D. Ćorić, High-speed internal strain measurements in composite structures under dynamic load using embedded FBG sensors, Compos. Struct. 92 (2010) 1905–1912.
[27] H. Kim, J. Yoon, H. Kim, J. Han, Measurement of the thermal expansion of space structures using fiber Bragg grating sensors and displacement measuring interferometers, Meas. Sci. Technol. 21 (2010), 085704.
[28] M. Mulle, A. Yudhanto, G. Lubineau, R. Yaldiz, W. Schijve, N. Verghese, Internal strain assessment using FBGs in a thermoplastic composite subjected to quasi-static indentation and low-velocity impact, Compos. Struct. 215 (2019) 305–316.
[29] G. Szebényi, Y. Blößl, G. Hegedüs, T. Tábi, T. Czigany, R. Schledjewski, Fatigue monitoring of flax fibre reinforced epoxy composites using integrated fibre-optical FBG sensors, Compos. Sci. Technol. 199 (2020), 108317.
[30] S. Mohanta, Y. Padarthi, S. Chokkapu, J. Gupta, S. Neogi, Ultra-violet health monitoring of smart composite laminate using embedded fiber Bragg grating

sensors, J. Compos. Mater. 54 (2020) 3143–3158.
[31] A.I. Gusarov, D.S. Starodubov, F. Berghmans, Design of a radiation-hard optical fiber Bragg grating temperature sensor, Proc. SPIE Int. Soc. Opt. Eng. 3872 (1999) 43–50.
[32] A.V. Faustov, A.I. Gusarov, P. Mégret, M. Wuilpart, D. Kinet, A.V. Zhukov, S.G. Novikov, V.V. Svetukhin, A.A. Fotiadi, Gamma radiation-induced blue shift of resonance peaks of Bragg gratings in pure silica fibres, Quant. Electron. 46 (2016) 150–154.
[33] S. Girard, J. Kuhnhenn, A. Gusarov, B. Brichard, M. Van Uffelen, Y. Ouerdane, A. Boukenter, C. Marcandella, Radiation effects on silica-based optical fibers: recent advances and future challenges, IEEE Trans. Nucl. Sci. 60 (2013) 2015–2036.
[34] A. Gusarov, S.K. Hoeffgen, Radiation effects on fiber gratings, IEEE Trans. Nucl. Sci. 60 (2013) 2037–2053.
[35] D. Kinet, C. Broadway, A. Gusarov, P. Mégret, C. Caucheteur, K. Kalli, S.O. O'Keeffe, G. Brambilla, Fibre Bragg gratings wavelength evolution and thermal sensitivity under gamma irradiation, in: Seventh European Workshop on Optical Fibre Sensors, Limassol, Cyprus, October 1-4, 2019.
[36] M.A.S. Zaghloul, M. Wang, S. Huang, C. Hnatovsky, D. Grobnic, S. Mihailov, M. Li, D. Carpenter, L. Hu, J. Daw, G. Laffont, S. Nehr, K.P. Chen, Radiation resistant fiber Bragg grating in random air-line fibers for sensing applications in nuclear reactor cores, Opt. Express. 26 (2018), 11775.
[37] J. He, B. Xu, X. Xu, C. Liao, Y. Wang, Review of femtosecond-laser-inscribed fiber Bragg gratings: fabrication technologies and sensing applications, Photonic Sensors. 11 (2021) 203–226.
[38] J. Chen, J. Wang, X. Li, L. Sun, S. Li, A. Ding, Monitoring of temperature and cure-induced strain gradient in laminated composite plate with FBG sensors, Compos. Struct. 242 (2020), 112168.
[39] A. Birri, B.A. Wilson, T.E. Blue, Deduced refractive index profile changes of type I and type II gratings when subjected to ionizing radiation, IEEE Sens. J. 19 (2019) 5000–5006.
[40] S.J. Mihailov, Fiber Bragg grating sensors for harsh environments, Sensors. 12 (2012) 1898–1918.
[41] H. Henschel, D. Grobnic, S.K. Hoeffgen, J. Kuhnhenn, S.J. Mihailov, U. Weinand, Development of highly radiation resistant fiber Bragg gratings, IEEE Trans. Nucl. Sci. 58 (2011) 2103–2110.
[42] A. Theodosiou, A. Leal-Junior, C. Marques, A. Frizera, A.J.S. Fernandes, A. Stancalie, A. Ioannou, D. Ighigeanu, R. Mihalcea, C.D. Negut, K. Kalli, Comparative study of γ- and e-radiation-induced effects on FBGs using different femtosecond laser inscription methods, Sensors. 21 (2021) 8379.
[43] A. Morana, S. Girard, E. Marin, C. Marcandella, S. Rizzolo, J. Perisse, J. Mace, A. Taouri, A. Boukenter, M. Cannas, Y. Ouerdane, Radiation vulnerability of fiber Bragg gratings in harsh environments, J. Lightwave Technol. 33 (2015) 2646–2651.
[44] L. Remy, G. Cheymol, A. Gusarov, Compaction in optical fibres and fibre Bragg gratings under nuclear reactor high neutron and gamma fluence, IEEE Trans. Nucl. Sci. 63 (2016) 2317–2322.
[45] Effect of kGy dose level gamma radiation on Ge-doped FBGs and femtosecond-laser-inscribed pure-silica-core FBGs, in: 16th International Conference on Optical Communications and Networks, Wuzhen, China, August 7-10, 2017.